# Analysis of the *Aspergillus fumigatus* Biofilm Extracellular Matrix by Solid-State Nuclear Magnetic Resonance Spectroscopy

Courtney Reichhardt[a], Jose A. G. Ferreira[b,c *], Lydia-Marie Joubert[d], Karl V. Clemons[b,c], David A. Stevens[b,c], and Lynette Cegelski[a#]

[a]Department of Chemistry, Stanford University, Stanford, California, USA; [b]Department of Medicine, Division of Infectious Diseases and Geographic Medicine, Stanford University, Stanford, California, USA; [c]California Institute for Medical Research, San Jose, California, USA; [d]Cell Sciences Imaging Facility, Stanford University School of Medicine, Stanford, California, USA

Running Head: Analysis of *A. fumigatus* ECM by Solid-State NMR

#Address correspondence to Lynette Cegelski, cegelski@stanford.edu

* Present address: School of Medicine, Faculdade de Saúde e Ecologia Humana-FASEH, Vespasiano, Brazil

CR and JAGF contributed equally to this work.

ABSTRACT

*Aspergillus fumigatus* is commonly responsible for lethal fungal infections among immunosuppressed individuals. *A. fumigatus* forms biofilm communities that are of increasing biomedical interest due to the association of biofilms with chronic infections and their increased resistance to antifungal agents and host immune factors. Understanding the composition of microbial biofilms and the extracellular matrix is important to understanding function and, ultimately, to developing strategies to inhibit biofilm formation. We implemented a solid-state NMR approach to define compositional parameters of the *A. fumigatus* extracellular matrix (ECM) when biofilms are formed in RPMI 1640 nutrient medium. Whole biofilm and isolated matrix networks were also characterized by electron microscopy, and matrix proteins were identified through protein gel analysis. The $^{13}C$ NMR results defined and quantified the carbon contributions in the insoluble ECM, including carbonyls, aromatic carbons, polysaccharide carbons (anomeric and non-anomerics), aliphatics, etc. Additional $^{15}N$ and $^{31}P$ NMR spectra permitted more specific annotation of the carbon pools according to C-N and C-P couplings. Assimilating these data, the *A. fumigatus* ECM produced under these growth conditions contains approximately 40% protein, 43% polysaccharide, 3% aromatic-containing components, and up to 14% lipid. These fundamental chemical parameters are needed to consider the relationships between composition and function in the *A. fumigatus* ECM and will enable future comparisons with other organisms and with *A. fumigatus* grown in alternate conditions.

## INTRODUCTION

*Aspergillus fumigatus* is the most important etiological agent of human aspergillosis and is recognized as a highly allergenic and opportunistic pathogen, causing acute and chronic infections particularly among immune-compromised individuals (1). Hospital-associated outbreaks of *A. fumigatus* may occur during periods of construction or renovation (2) or when fungi can colonize water distribution systems that then lead to spore aerosolization in patient care areas and patient exposure (1). Additionally, *A. fumigatus* can cause infections as a result of colonizing medical implant devices, including cardiac pacemakers, joint replacements, and breast implants (3). Despite improvements in diagnostics and the antifungal armamentarium, including broad-spectrum azoles and the echinocandin antifungals, mortality due to *A. fumigatus* invasive infections remains high.

Like many microorganisms, *A. fumigatus* can also assemble into multicellular communities, termed biofilms, composed of cells plus an extracellular matrix (ECM)(4-9). Although more work is needed to fully understand the functional implications of biofilm formation by *A. fumigatus*, recent evidence suggests that the ECM may provide the infrastructure for enhancing cell density, controlling disaggregation, and altering nutritional needs, as well as providing a protective physical and chemical barrier that can decrease sensitivity to competitors and to antifungal drugs and the immune response (10). Understanding the composition of microbial biofilms and the ECM is important for considering functional differences among biofilm formers and, ultimately, to developing strategies to inhibit biofilm formation. Valuable detail has been obtained for many biofilms regarding macroscopic properties and the identification of key matrix parts (5, 7), but quantitative compositional detail remains sparse in most biofilm systems (11).

69 Mature *A. fumigatus* biofilms have been observed as three-dimensional assemblies between 10
70 µm and 200 µm thick. The putative parts list for the *A. fumigatus* ECM includes polysaccharides
71 (galactomannon, galactosaminogalactan, α-1,3 glucans, and monosaccharides), proteins (major
72 antigens and hydrophobins), melanin, and extracellular DNA (8). These identifications primarily
73 relied upon immunoassays, yet suggested compositions vary depending upon growth conditions
74 and analysis methods. Attempts to generate quantitative descriptions of the *A. fumigatus* ECM
75 have been limited to the soluble or small molecular weight components of the ECM. Indeed, the
76 insoluble and complex nature of the ECM of most biofilms has posed a challenge to analysis by
77 traditional techniques, which generally rely on dissolution of matrix parts and solution-based
78 methods such as HPLC-mass spectrometry, protein analyses, and solution nuclear magnetic
79 resonance (NMR) to examine soluble parts. Estimates are sometimes made regarding relative
80 quantities of these components in the intact matrix. However, the inability to completely
81 solubilize ECM components and the possible perturbations or degradation of material that can
82 occur during sample preparation can severely compromise estimates of composition for the intact
83 ECM. Thus, despite the prevalent roles that biofilms play in human infection, there has been
84 little reliable quantitative information available regarding biofilm matrix composition.
85
86 Solid-state NMR spectroscopy is uniquely suited to study complex and insoluble biological
87 materials (12) such as whole cells (13-18), biofilms, and the extracellular matrix (19-22). Solid-
88 state NMR approaches can be used to quantify composition and to measure internuclear
89 distances to determine parameters of architecture in such macromolecular assemblies and does
90 not require soluble or crystalline samples (15). We recently introduced two approaches to define
91 the composition of the insoluble ECM of bacterial biofilms using solid-state NMR integrated

92 with complementary biochemical analysis and electron microscopy. Both approaches involve a
93 panel of one-dimensional NMR experiments, which can be employed on any spectrometer
94 equipped to perform solid-state NMR measurements. In the case of a uropathogenic *E. coli*
95 biofilm that assembles an amyloid-associated ECM, we employed a bottom-up approach and
96 discovered that the spectral addition of only two separate samples corresponding to separate
97 isolated biofilm parts, (i) curli amyloid fibers and (ii) a modified form of cellulose, in a 6:1 ratio,
98 were able to completely recapitulate the spectrum of the intact ECM (20). This was the first
99 quantitative determination of the composition of an intact ECM preparation. In this approach,
100 one requires separate samples of putative biofilm parts for analysis, and these are not readily
101 available for many biofilm systems. Thus, while working with the more compositionally
102 complex biofilms formed by *Vibrio cholerae*, we developed a top-down methodology that could
103 be applied to other biofilm systems with only the complex ECM material to examine (21). In the
104 top-down approach, carbon contributions are assigned by type of chemical functionality (e.g.,
105 carbonyls, aromatics, anomerics) and quantified by peak integrals. If $^{15}N$ labeling of the growth
106 medium is possible, then nitrogen pools can also be examined. In addition, the carbons can be
107 more specifically annotated through $^{13}C$-$^{15}N$ recoupling experiments to determine, for example,
108 what percentage of carbonyls may be part of peptide bonds versus non-nitrogen bonded
109 carbonyls. Together, the analysis of the *V. cholerae* biofilm formed on a minimal agar medium
110 revealed a complex ECM dominated by highly modified polysaccharides, with additional
111 contributions from lipids and proteins.
112
113 Here we provide our analysis of the biofilm composition of the filamentous fungus *A. fumigatus*
114 grown in RPMI 1640 medium, a medium commonly employed for mammalian cell culture,

using the top-down methodology that requires only the complex matrix material isolated from the hyphae. We integrated electron microscopy, protein gel and protein identification, and quantitative solid-state NMR measurements involving $^{13}C$, $^{15}N$, and $^{31}P$ nuclei to characterize the *A. fumigatus* biofilm. In order to permit $^{15}N$ NMR measurements, we generated a fully $^{15}N$-labeled version of RPMI 1640 medium. Collectively, we provide a general spectral accounting of the carbon, nitrogen, and phosphorous content and provide a detailed analysis of the carbon pools in the *A. fumigatus* ECM.

## MATERIALS AND METHODS

***Aspergillus* growth and ECM extraction.** A standardized *Aspergillus fumigatus* suspension was inoculated in each of five 500-ml polystyrene tissue-culture flasks containing 100 ml of RPMI 1640 medium (final concentration of $10^5$ conidia/ml) and incubated at 37 °C for 96 h. To generate a fully $^{15}N$-labeled version of RPMI 1640, all amino acids were replaced by 0.674 g/L $^{15}N$ labeled algal amino acid mixture (Aldrich Cat # 608947). The algal extract contains between 65-95% amino acids by mass and has an isotope enrichment of 99% for $^{15}N$. For uniformly $^{15}N$-labeled samples, $Ca(NO_3)_2$ (98% $^{15}N$ enrichment) was also used in place of its unlabeled counterpart. Harvested biofilms were washed in situ twice with 100 ml of PBS to remove planktonic and loosely adherent cells. The sessile cells were then flooded with 40 ml of 10 mM Tris (pH 7.4) per flask and mixed mildly with a vortex mixer for 60 s. Each sample was transferred to a 50 ml conical tube and stored at 4°C until processing.

137 For the ECM extraction, the tubes containing the *A. fumigatus* biofilm were subjected to
138 sonication (Fisher Scientific, model FB505, amplitude of 20%) for 10 min, followed by high-
139 speed mixing on a vortex mixer for 30 s. The tubes were then centrifuged at 3600 x *g* at 4 °C for
140 15 min. The supernatant was poured into new tubes and centrifuged again to remove additional
141 cells. The resulting supernatant was dialyzed against distilled water for 2 days (3.5 kD molecular
142 weight cut-off (MWCO)). The supernatant was flash frozen in liquid nitrogen and lyophilized.
143
144 **Electron microscopy.** Negative staining transmission electron microscopy (TEM) was
145 performed on ECM samples. Samples were applied to 300-mesh copper grids coated with
146 Formvar film (Electron Microscopy Sciences, Hatfield, PA) for 2 min and then rinsed in
147 deionized water. The samples were negatively stained with 2% aqueous uranyl acetate for 90 s,
148 excess stain was wicked off with filter paper, and then the sample was air-dried. Microscopy
149 was performed with a JEM-1400 (JEOL, LLC) operated at 120 kV. For scanning electron
150 microscopy (SEM) analysis, *Aspergillus* biofilms were suspended in 10 mM Tris (pH 7.4), fixed
151 for 45 mins with 4% paraformaldehyde and 2% glutaraldehyde in 0.1M sodium cacodylate
152 buffer (pH 7.2), rinsed in the same buffer and post-fixed for 45 mins with 1% aqueous $OsO_4$.
153 After dehydration in an ascending ethanol series (50, 70, 90, 100 % (twice); 5 min each) samples
154 were gently vacuum-filtered onto 0.2 and 0.45 um polyamide filters (Sartorius, Bohemia, NY)
155 kept under a steady stream of 100% ethanol. Samples were then critical point dried with liquid
156 $CO_2$ in a Tousimis Autosamdri-815B apparatus (Tousimis, Rockville, MD), mounted onto
157 double-sided copper tape on 15 mm aluminum stubs (Electron Microscopy Sciences, Hatfield,
158 PA), and sputter-coated with 50Å of gold-palladium using a Denton Desk II Sputter Coater
159 (Denton Vacuum, Moorestown, NJ). Visualization was performed with both a Hitachi S-3400N

SEM (Hitachi HTA, Dallas, TX) operated at 10-15kV using Everhart Thornley SE (Secondary Electron) detection, and a Zeiss Sigma FESEM (Carl Zeiss Microscopy, Thornwood, NY) operated at 2kV, using InLens SE detection at working distance 4-5mm. Images were captured in TIFF using store resolution 2048x1536 and a line averaging noise reduction algorithm.

**SDS-PAGE protein analysis and identification.** Lyophilized ECM was suspended in SDS-PAGE sample buffer containing 8 M urea and 50 mM DTT and used for electrophoresis in a 4-20% gradient Tris-Glycine SDS-PAGE gel (Novex). For Edman degradation (UC Davis Proteomic Core), samples were transferred to a PVDF membrane and were loaded onto an ABI Procise sequencer and subjected to Edman degradation. In this processing, for each residue/cycle, the free N-terminus of each immobilized protein was coupled with phenyl isothiocyanate, cleaved with trifluoroacetic acid, and then converted to the more stable phenylthiohydantion amino acid derivative which was separated by reverse phase chromatography and detected by UV-Vis spectrophotometry.

**Solid-state NMR.** All solid-state NMR experiments were performed using an 89-mm wide-bore Varian magnet at 11.7 T (499.12 MHz for $^{1}$H, 125.52 MHz for $^{13}$C, and 50.58 MHz for $^{15}$N) and an 89-mm wide-bore Agilent magnet at 11.7 T (500.92 MHz for $^{1}$H, 125.97 MHz for $^{13}$C, 50.76 MHz for $^{15}$N, and 202.78 MHz for $^{31}$P), Varian/Agilent consoles, and home-built four-frequency transmission-line probes with a 13.66 mm long, 6 mm inner-diameter sample coil and a Revolution NMR MAS Vespel stator. Samples were spun in thin-wall 5 mm outer-diameter zirconia rotors (Revolution NMR, LLC) at 7143±2 Hz, using a Varian MAS control unit. The temperature was maintained at -10°C. For all NMR experiments, π-pulse lengths were 7 μs for







Eukaryotic Cell

$^{1}$H and 10 μs for $^{13}$C, $^{15}$N, and $^{31}$P. Proton-carbon and proton-nitrogen cross-polarization occurred at 50 kHz for 1.5 ms unless otherwise noted. Proton dipolar coupling was performed at 90 kHz with two-pulse phase-modulation (TPPM). For all experiments, the recycle delay was 2s. The $^{13}$C spectra were referenced to tetramethylsilane (TMS); $^{15}$N spectra were referenced to liquid ammonia; and $^{31}$P spectra were referenced to phosphoric acid. All chemical shift references were determined relative to an adamantane standard. Rotational-echo double-resonance (REDOR) dephasing was calculated using peak integral values. Multi-peak fitting and integration was performed in software written for Igor Pro (WaveMetrics, Lake Oswego, OR, USA).

## RESULTS

***A. fumigatus biofilm formation and ECM isolation and protein analysis.*** A biofilm contains both microbial cells and their secreted extracellular matrix (ECM)(23). The *A. fumigatus* biofilm was visualized by scanning electron microscopy (SEM) (Figure 1A-C). The biofilm hyphae are densely packed and connected to one another by tightly woven webs of ECM. The ECM also appears as fibrous and granular networks coating the individual hyphae (Figure 1C). The biofilms are similar in appearance to the *A. fumigatus* biofilms grown in aerial static cultures reported by Beauvais *et al*.(5), with some ECM material covering individual hyphae and some serving to glue hyphae together into a contiguous network. To examine the ECM separately from the hyphae, we developed a minimally perturbative ECM extraction protocol that included sonication to disrupt the biofilm and subsequent centrifugation to separate the hyphae from the ECM. The extracted ECM was best imaged by transmission electron microscopy (TEM), which

revealed aggregative material, including fibrous strands and vesicle-type structures (Figure 1D). SDS-PAGE analysis of the ECM yielded bands corresponding to several SDS-soluble proteins of different molecular weights (Figure 1C). Gel bands corresponding to the proteins that were in relatively high abundance were excised and analyzed by mass spectrometry and Edman sequencing for protein identification. Although proteins may escape detection by PAGE analysis if they are not soluble and not able to run into the gel, this analysis at least allowed for the identification of the proteins that could be detected to help characterize the ECM preparation and to be sure that cellular contaminants were not associated with the preparation. Two unique proteins, Catalase B and Asp f2 (major allergen), were identified by mass spectrometry and by Edman degradation and have molecular weights of 79,910 Da (Band 1, Catalase B) and 32,838 Da (Band 2, Asp f2). Importantly, both proteins are typically secreted from cells and found at or beyond the cell surface of *A. fumigatus* (24-26). Both proteins are N-linked glycosylated, and digestion with PNGase enhanced the intensity of Band 3 while depleting Band 2 intensity (Figure S1). By Edman degradation, the protein in Band 3 also contained the same N-terminal amino acids as Asp f2. Thus, Band 3 represents deglycosylated Asp f2. Band 4 is a truncated form of Catalase B, with the N-terminus corresponding to residue 334 from the full-length protein sequence (determined by Edman degradation analysis). The protein in Band 5 appears to be Asp f2, containing the same N-terminus as full-length Asp f2. It may appear at a lower apparent molecular weight due to an altered glycosylation pattern or it may have a truncated C-terminus.

***Spectral comparisons of intact A. fumigatus biofilms (cells plus matrix) and the isolated ECM.*** To obtain quantitative detail of the *A. fumigatus* ECM composition, we employed a top-down

229 solid-state NMR approach as described in the Introduction, which does not depend upon sample
230 solubility or crystallinity. A standard way to obtain a carbon spectrum by solid-state NMR
231 spectroscopy is through cross-polarization magic-angle spinning (CPMAS), introduced in 1976
232 (27,28). During CPMAS, carbon magnetization is enhanced through spin polarization contact
233 with an abundant $^{1}H$ spin lattice, present in nearly all biomaterials (28), and the sample is
234 mechanically spun at the magic-angle to help suppress dipolar couplings and chemical shift
235 anisotropy that would broaden the resonances significantly. The $^{13}C$ CPMAS spectrum of the
236 intact *A. fumigatus* biofilm containing hyphae plus associated ECM has strong polysaccharide
237 peaks (anomerics, 100-105 ppm; ring-sugar carbons, 60-85 ppm), consistent with the presence of
238 chitin and additional polysaccharides associated with the thick hyphal cell walls (Figure 2)(7,
239 29,30). The $^{13}C$ CPMAS spectrum of the extracted ECM reveals a different profile of carbon
240 pools reflective of its composition. The ECM spectrum contains carbon chemical shifts that are
241 representative of proteins (carbonyl, 173 ppm; α-carbons, 50-60 ppm; glycine α-carbons, 38-43
242 ppm); other aliphatics (10-35 ppm), polysaccharides (anomeric carbons, 97-103 ppm; ring-sugar
243 carbons, 60-85 ppm), lipids (24, 33, and 173 ppm), and aromatic compounds (130-160 ppm)
244 (Figure 2B). Relative intensities differ between the intact biofilm and ECM spectra. In addition,
245 the polysaccharide peaks of the ECM sample exhibit a slight upfield shift with respect to those of
246 the biofilm sample, indicative of a difference in carbohydrate composition or local chemical
247 environment. The differences between the spectra of the biofilm and extracted ECM, together
248 with the protein gel and EM characterization of the ECM, suggest that the ECM extraction
249 resulted in a material free of hyphal contamination.
250

To use peak integrals or peak heights from CPMAS spectra quantitatively, one must account for the possibility that some carbons might exhibit differences in cross-polarization efficiency or relaxation. Thus, CPMAS spectra were obtained as a function of CP time, where normalized intensities could be obtained based on possible differences due to CP (Figure S2). Nearly all carbons exhibited similar CP behavior with differences noted in some aliphatic carbons. The polysaccharide anomeric carbons and associated ring sugar carbons are a prominent spectral feature and account for approximately 43% of the total carbon mass. The relative contributions of other spectral regions within the $^{13}C$ spectrum are fully outlined in Table 1 after all the carbon pools were first more fully annotated using additional NMR measurements described below.

To assess possible compositional variation between different biofilm samples and ECM extractions, we collected $^{13}C$ CPMAS spectra of two separately cultured biofilm samples and their corresponding identically prepared ECM samples (Figure 3). The major differences between samples obtained from the two separate cultures occur in peaks uniquely attributed to polysaccharides, and changes in overall polysaccharide content in the intact biofilms were similarly present in the corresponding extracted ECM preparations. As anticipated, ECM extracted from biofilms with high overall polysaccharide content also had greater polysaccharide content. In the ECM samples, the percentage of carbon that is attributed to polysaccharide ranges from 20 to 43% of the total carbon mass. Therefore, differences in ECM composition could be attributed to biological variability in biofilm production and not necessarily to differences in ECM extraction. The fact that the polysaccharide carbons increase without associated increases in carbonyls or α-carbons indicates that these polysaccharides are not significantly modified unlike the more complex *Vibrio* polysaccharide (VPS) that contains extensive acetyl and glycine

modifications (21). The observed variability in the *A. fumigatus* ECM polysaccharide content is in contrast to what we have previously observed for *E. coli* ECM, which maintains a nearly constant ratio of 6:1 protein to polysaccharide for samples grown in the same way(20). Thus, we speculate that there may be more flexibility in the range of polysaccharide required to permit biofilm formation in biofilms with relatively high polysaccharide content. All subsequent NMR experiments and analyses were performed on the biofilm and corresponding ECM samples with greater polysaccharide content.

The $^{15}$N CPMAS spectrum of *A. fumigatus* biofilm contains a prominent peak centered at 122 ppm as well as peaks corresponding to multiple amine types and amino acid sidechains (Figure 2). In contrast, the $^{15}$N CPMAS spectrum of the ECM contains a single prominent amide signal centered at 119 ppm, which is upfield of the amide peak in the biofilm spectrum, encompassing 90% of the total integrated spectral area (Figure 2). The quantitative $^{15}$N spectral contributions were also determined by analysis of CPMAS spectra obtained as a function of CP time (Figure S3). Amides are present in all peptides, some amino acid sidechains, and can be present as modifications among other biomolecules, e.g. N-acetyl modifications. The $^{15}$N peaks at 34 and 40 ppm correspond to amines, such as those present in the sidechain of lysine and those present as amino modifications of other biomolecules. Together, the amines in the ECM account for 4% of the nitrogen spectral area. The $^{15}$N peaks at 73 and 84 ppm correspond to the sidechain nitrogens of arginine, and together account for 4% of the spectral area of the ECM. The spectrum also contains a peak at 174 ppm, where imidazole nitrogens in histidine sidechains would appear, and accounts for 2% of the ECM spectrum.

297 ***Detailed analysis of the A. fumigatus ECM carbon pools using $^{13}C\{^{15}N\}$REDOR NMR.*** Protein
298 carbonyls and α-carbon chemical shifts appear at 173 and 50-60 ppm, respectively. However,
299 carbons from other biomolecular groups may also contribute to these spectral regions. Proteins
300 contain amino acids with α-carbons and carbonyls that are each directly bonded to nitrogen, and
301 based upon the uniqueness of these carbon-nitrogen pairs, we are able to spectroscopically select
302 and determine the relative amounts of nitrogen-bonded carbonyls and α-carbons within a carbon
303 spectrum of a complex material. To quantify the relative contribution of proteins to the ECM, we
304 employed $^{13}C\{^{15}N\}$REDOR with 1.6 ms dephasing to select directly bonded $^{13}C$-$^{15}N$ pairs
305 (Figure 4, left). REDOR experiments are done in two parts: one reference spectrum is collected
306 without dephasing pulses ($S_0$) and one "dephased" spectrum is collected with rotor-synchronized
307 dephasing pulses (S) to reintroduce the dipolar couplings that are suppressed during magic-angle
308 spinning (31). The difference spectrum (ΔS) is obtained from the subtraction of the S spectrum
309 from the $S_0$ spectrum. Only carbons that are proximate to the dephasing spin contribute to
310 intensities in the ΔS spectrum. In the case of $^{13}C\{^{15}N\}$REDOR with 1.6 ms dephasing, the ΔS
311 spectrum reports on those carbons directly bonded to nitrogen. At longer dephasing times, one
312 can extend this ruler to examine longer range C-N contacts.
313
314 In the $^{13}C$ CPMAS spectrum of *A. fumigatus* ECM, the carbonyl peak accounts for 12% of the
315 carbon, and it exhibited 76% dephasing in the one-bond $^{13}C\{^{15}N\}$REDOR measurement. Thus, at
316 most, only 76% of all carbonyl carbons are directly bonded to nitrogen, which indicates that 9%
317 of the total $^{13}C$ CPMAS spectral area can be assigned to nitrogen-bonded carbonyls (76% of
318 12%). Carbonyl-nitrogen pairs occur in peptide bonds of proteins as well as in N-acetyl groups.
319 Glycine α-carbons appear near 40 ppm, while all the other α-carbons contribute to the resonances

centered at 55 and 60 ppm. Other chemical species can also contribute to these spectral regions, and examples include the C6 carbons of hexose-based polysaccharides. Thus, the REDOR measurement is used to quantify the percentage of these carbons that are adjacent to a nitrogen and thus can be attributed to α-carbons. The integrals of the resonances at 55 and 60 ppm together account for 14% of the total $^{13}C$ CPMAS spectral area (Figure 2), and the region exhibited 52% dephasing. Thus, we can place an upper limit on the carbon mass that can be attributed to protein α-carbons as 7% (52% of 14%). The region near 40 ppm exhibited 30% dephasing, suggesting that 0.3% of the total carbon mass is due to glycyl α-carbons. The approximate 1:1 ratio of the numbers of nitrogen-bonded carbonyls (9%) to α-carbons (7%) is consistent with that expected for protein, and the 1:23 ratio of glycine α-carbons (0.3%) to other α-carbons (7%) is also within expectations for the composition of average proteins. The slight 2% excess of nitrogen-bonded carbonyls relative to α-carbons would be consistent with the presence of nitrogen-bonded carbonyls in N-acetyl modifications.

The extent to which carbons were within a longer, approximately 2.5 Å proximity to a nitrogen was examined using $^{13}C\{^{15}N\}$REDOR with an evolution time of 8.95 ms (Figure 4, right). As expected, the carbonyl and α-carbon regions exhibited additional dephasing. The $CH_2$ region centered at 33 ppm accounts for 10% of the total carbon spectral area and exhibited 16% dephasing. The $CH_2$ carbons that are spatially close to nitrogen encompass 3% (16% of 10%) of all carbons and can be accounted for by amino acid sidechains, especially those that also contain sidechain nitrogen including arginine, glutamine, and lysine. The remaining intensity at 33 ppm can be attributed to the aliphatic CH2 groups of lipids, and accounts for 7% of the total carbon mass. Dephasing in the aliphatic regions (12-35 ppm) also was observed, indicative of the

343 presence of amino acid sidechains and possible N-acetyl modifications. The 12-25 ppm region,
344 which includes methyl groups such as those in amino acids, acetyl modifications, and termini of
345 fatty acids, constitutes 18% of the total $^{13}C$ CPMAS spectral area and exhibited 27% dephasing,
346 suggesting that 5% (27% of 18%) of carbons belong to sidechains of amino acids such as alanine
347 or exist as methyl groups of N-acetyl modifications. The observed 12% dephasing of the 72-ppm
348 sugar peak further supports the presence of N-acetyl modifications of polysaccharides such those
349 in galactosaminogalactan (4), which was previously shown to be a component of the *A.*
350 *fumigatus* ECM, or in the N-acetylglucosamine (GlcNAc) moieties involved in N-linked
351 glycosylation of some *A. fumigatus* extracellular proteins.
352
353 ***$^{13}C$-$^{31}P$ couplings indicate the presence of phosphorus-containing biomolecules in the ECM.***
354 To examine the possibility that phosphorus-containing biomolecules contribute to *A. fumigatus*
355 ECM, we performed $^{31}P$ NMR experiments. The ECM $^{31}P$ CPMAS spectrum (Figure 5A)
356 contained a broad resonance that could be fit by three peaks centered at -7, -0.4, and 2 ppm
357 (Figure S4), with the corresponding sidebands separated by the MAS spinning frequency. These
358 $^{31}P$ shifts could be due to a multitude of phosphorylated biomolecules including lipids, proteins,
359 sugars, or nucleic acids. To better evaluate possible origins of phosphorous contributions to the
360 ECM, we performed $^{13}C\{^{31}P\}$REDOR with 8.95 ms dephasing to identify any carbons that were
361 proximate to phosphorous (Figure 5B). With this one long-range REDOR evolution time, the
362 measurement serves as a qualitative analysis that could identify the presence of a few C-P
363 contacts in close proximity (within 6Å) or many C-P contacts at longer range (>6Å). We
364 observed dephasing by phosphorous of the carbon peaks centered at 60, 72, and 80 ppm as well
365 as the carbonyl peak at 173 ppm (Figure 5B, dashed REDOR difference spectrum, ΔS).

366 Biomolecules that contain phosphorus atoms that are spatially close to carbons with chemical
367 shifts near 60-80 ppm include nucleic acids (phosphorylated ribose), phospholipids,
368 phosphorylated sugars, and proteins that are phosphorylated on serine or threonine residues. The
369 dephasing of the carbonyl peak by phosphorus is consistent with phospholipid and
370 phosphorylated proteins(21, 32). If the only phosphorus-containing molecules in the ECM were
371 phospholipids, we would have observed dephasing of the 33-ppm peak corresponding to lipid
372 aliphatics. Similarly, phosphorylated proteins could only account for a fraction of the total
373 $^{13}C\{^{31}P\}$REDOR ΔS spectrum, even if every threonine and serine in the identified ECM
374 proteins, Catalase B and Asp f2, were phosphorylated. Thus, it is possible that multiple types of
375 biomolecules contribute to the phosphorus pools of *A. fumigatus* ECM.
376
377 **DISCUSSION**
378 Our integrated solid-state NMR, electron microscopy, and biochemical analysis of the
379 composition of the *A. fumigatus* ECM extracted from cells grown in RPMI 1640 medium
380 provide insight into the identification and contributions of biomolecules present in the ECM.
381 Electron micrographs of the *A. fumigatus* biofilm revealed sheets of ECM that connected some,
382 but not all, of the hyphae in the dense community of cells (Figure 1). The ECM also served to
383 coat some of the hyphae giving them a rough and granular web-like appearance. Inspection by
384 electron microscopy is invaluable in revealing biofilm architecture and in characterizing the
385 extracted ECM, but does not provide insight into chemical and molecular composition. The $^{13}C$
386 NMR results defined the quantities of carbon types, including carbonyls, aromatic carbons,
387 polysaccharide carbons (anomeric and non-anomerics), and aliphatics, present in the insoluble
388 ECM material. The $^{15}N$ and $^{31}P$ NMR spectra provided additional detail regarding nitrogen and

389 phosphorous pools in the ECM. Furthermore, by ensuring full incorporation of $^{15}N$ labels into the
390 sample, we were able to further refine and quantify specific types of carbons, including one-bond
391 C-N pairs, such as those in peptide carbons and alpha carbons. The full definition of the carbon
392 pools were summarized in Table 1 and provide the absolute atomic-level parameters of the ECM
393 obtained directly from the NMR measurements. Assimilating these data as discussed further
394 below, we find that the *A. fumigatus* ECM at the molecular level contains approximately 40%
395 protein, 43% polysaccharide, 3% aromatic-containing components, and at least 7% lipid.
396 Additionally, we identified the presence of phosphorus-containing biomolecules in the ECM,
397 although we were unable to specifically annotate them in this study.
398
399 Polysaccharides (anomerics and ring sugars) account for approximately 43% of the total ECM
400 carbon mass (Figure 2, Figure S2, and Table 1) although variability in polysaccharide content
401 between separate cultures was observed (Figure 3) and a second sample was reduced in its
402 polysaccharide content (with sugar carbons representing 20% of the carbon mass). Thus,
403 biologically, the *A. fumigatus* ECM exhibits variation in the range of polysaccharide production
404 during biofilm formation in comparable conditions. This is unlike *E. coli*, where under given
405 growth conditions, the insoluble ECM composition exhibits very little variability (85-87% curli
406 protein and 13-15% modified cellulose), although the ECM purification procedures are not
407 identical for the two organisms. The *A. fumigatus* NMR results are consistent with
408 polysaccharides previously reported to be present in *A. fumigatus* biofilm, which include
409 galactomannan, galactosaminogalactan, α-1,3 glucans, and monosaccharides.
410 Galactosaminogalactan, which is a polymer of galactose and N-acetylglucosamine, plays a
411 critical role in the adherence and virulence of *A. fumigatus* (33), and the presence of N-acetyl

412 modifications, such as occur in galactosaminogalactan, was supported by the $^{13}C\{^{15}N\}$REDOR
413 analyses.
414
415 Protein accounts for approximately 40% of the total ECM carbon mass. This estimation stems
416 from the absolute NMR determination that amino acid α–carbons and nitrogen-bonded carbonyls
417 account for 7% and 9% of the carbon mass, respectively. Amino acids contain an average of 5.4
418 carbons and, thus, three additional carbons, on average, can be attributed to protein and would
419 contribute broadly to the aliphatic spectral region, consistent with what is observed (Figure 2). In
420 addition, the $^{15}N$ CPMAS (Figure 2) spectrum and the $^{13}C\{^{15}N\}$REDOR results (Figure 4)
421 suggest that most nitrogen is present in protein, and that there is very little nitrogen that exists as
422 modifications to other biomolecules. Protein gel analysis identified Catalase B and Asp f2 as the
423 major proteins in the ECM. Asp f2 has been associated with damage to the host epithelium and
424 host inflammatory reactions during fungal colonization (26). Accumulation of Catalase B in the
425 ECM of *A. fumigatus* biofilms has been detected by immunolabeling assays (5, 34), and catalase
426 is reported to play a critical role in other microbial biofilms including those formed by
427 *Pseudomonas aeruginosa* (35). The presence of Catalase B in the ECM is also consistent with its
428 protective role against reactive oxygen species, specifically hydrogen peroxide, which microbes
429 may encounter during infection of a host. Increased catalase production generally reduces the
430 susceptibility of microorganisms to phagocytosis and killing (36,37). Finally, it was previously
431 reported that the *A. fumigatus* ECM contained 2% (w/w) protein, which was determined using
432 the colorimetric Bradford assay (5). We similarly performed a BCA protein assay to determine
433 protein concentration. Using this colorimetric assay, we found the ECM to contain an apparent
434 estimate of 18% (w/w) protein. We know from the NMR results that this value is an

435 underestimate of the protein concentration and is likely due to inaccessibility of protein peptide
436 bonds within the matrix to reduce $Cu^{2+}$ ions in the BCA assay or due to complexation of $Cu^{2+}$ by
437 other components. This finding provides another example of how solution-based methods,
438 particularly such chemical reaction assays used for proteins within a complex mixture can fail to
439 quantify composition in intact and insoluble materials such as the *A. fumigatus* ECM.
440
441 For the final accounting, according to carbon mass, an additional 3% of the carbon mass was
442 attributed to aromatic molecules such as melanin (130-160 ppm). The presence of melanin in *A.*
443 *fumigatus* and other fungi is considered to be important for virulence because it affects the
444 immune response to fungal infection (38). We observe some dephasing in the aromatic carbon
445 region in the $^{13}C\{^{15}N\}$REDOR experiments that is consistent with melanin (example structure in
446 Table 1)(39,40), but due to the overlap of $^{15}N$ chemical shifts of amides and indoles (near 120
447 ppm) in the $^{15}N$ spectrum, it is not possible to unambiguously identify whether the indole
448 nitrogens are specifically attributed to melanin. The remaining 14% of the $^{13}C$ CPMAS spectral
449 area contains additional carbonyls (excluding nitrogen-bonded carbonyls already accounted for)
450 and aliphatics, with the presence of sharp $CH_2$ peaks, consistent with lipid molecules. Thus, the
451 ECM contains at least 7% lipid due to aliphatic $CH_2$ groups and up to 14% lipid total. The
452 carbonyl dephasing by phosphorous in the $^{13}C\{^{31}P\}$REDOR experiment (Figure 5) also suggests
453 that *A. fumigatus* ECM contains some phospholipids. There is no evidence for a prominent
454 contribution from nucleic acids in the *A. fumigatus* ECM characterized here, as the $^{13}C$ CPMAS
455 spectrum contains minimal contributions to aromatic regions and the $^{15}N$ spectrum lacks peaks
456 corresponding to nucleic acid $^{15}N$ chemical shifts. It is possible that this lack of nucleic acids is
457 due to the age of the biofilm when harvested and that older more mature biofilms would have

nucleic acids present in higher concentration. The lack of nucleic acids in our samples also indicates that the fungal biofilm is not necessarily dependent on nucleic acids for structural integrity as electron microscopy revealed the anticipated elaboration of ECM around and between the hyphae (41).

Thus, we determined the ECM composition of *A. fumigatus* to be approximately 40% protein, 43% polysaccharide, 3% aromatic compounds such as melanin, and up to 14% lipid. The ECM composition of *A. fumigatus* can be richer in polysaccharides than the ECM composition reported for *Candida albicans* with 55% protein, 25% carbohydrate, 15% lipid, and 5% nucleic acid (24). The analysis of the *Candida albicans* matrix material, however, used different chemical and solution-based methods to estimate matrix parts. Carbohydrate content was determined colorimetrically using a phenol-sulfuric acid precipitation protocol; protein concentration was determined using a BCA assay; lipids were extracted in organic solvent and analyzed by HPLC-mass spectrometry; and nucleic acid concentration was estimated by absorbance at 260 nm. Mass spectrometry, in particular, is invaluable in the specific identification of matrix components, but the overall modeling of the intact matrix composition and quantification from the analysis of soluble parts is limited. Our top-down NMR approach to characterize the ECM composition enables quantitative analysis. The NMR approach only required preparation of a uniformly $^{15}$N-labeled *A. fumigatus* sample with extraction of the ECM and no harsh hydrolyses, degradative measures, or caveats associated with attempting to quantify parts using solution-based assays that are subject to sampling bias and errors. Protein gel analysis provides a qualitative evaluation of the relative quality of the ECM preparation (detecting no contaminating intracellular proteins) and can identify the proteins in the ECM that are soluble

and can be accessed and compared among samples, for example. The NMR analysis should also be coupled with microscopy to provide visual inspection of the biofilm and ECM.

In summary, our analyses provide fundamental atomic-level compositional parameters in the complex ECM needed to consider the relationship between composition and function in the *A. fumigatus* ECM. Future comparisons with the ECM analysis of *A. fumigatus* in other growth conditions and with ECM from other strains will enable us to further build such composition-function relationships.

**ACKNOWLEDGMENTS**

This research was supported in part by the NIH Director's New Innovator Award to LC (DP2OD007488). We also acknowledge funding from the Child Health Research Institute, Stanford Transdisciplinary Initiatives Program (DAS) and a gift from Mr. John Flatley (DAS). CR is supported by the Althouse Stanford Graduate Fellowship and JAF has been partially supported by the Programa Ciencias sem Fronteiras CsF/ CNPq (Brazilian National Research Council). We acknowledge support from the Cell Sciences Imaging Facility at Stanford (NIH grant number 1S10RR02678001) for electron microscopy access.

**REFERENCES**

1. **Latge JP.** 2001. The pathobiology of *Aspergillus fumigatus*. Trends Microbiol **9:**382-389.

2. **Haiduven D.** 2009. Nosocomial aspergillosis and building construction. Med Mycol **47:**S210-216.

3. **Rosenblatt WB, Pollock A.** 1997. *Aspergillus flavus* cultured from a saline-filled implant. Plast Reconstr Surg **99:**1470-1472.

4. **Muller F-MC, Seidler M, Beauvais A.** 2011. *Aspergillus fumigatus* in the clinical setting. Med Mycol **49:**S96-S100.

5. **Beauvais A, Schmidt C, Guadagnini S, Roux P, Perret E, Henry C, Paris S, Mallet A, Prevost MC, Latge JP.** 2007. An extracellular matrix glues together the aerial-grown hyphae of *Aspergillus fumigatus*. Cell Microbiol **9:**1588-1600.

6. **Beauvais A, Loussert C, Prevost MC, Verstrepen K, Latge JP.** 2009. Characterization of a biofilm-like extracellular matrix in FLO1-expressing *Saccharomyces cerevisiae* cells. FEMS Yeast Res **9:**411-419.

7. **Beauvais A, Fontaine T, Aimanianda V, Latge JP.** 2014. *Aspergillus* cell wall and biofilm. Mycopathologia **178:**371-377.

8. **Kaur S, Singh S.** 2014. Biofilm formation by *Aspergillus fumigatus*. Med Mycol **52:**2-9.

9. **Mowat E, Butcher J, Lang S, Williams C, Ramage G.** 2007. Development of a simple model for studying the effects of antifungal agents on multicellular communities of *Aspergillus fumigatus*. J Med Microbiol **56:**1205-1212.

10. **Manavathu EK, Vager DL, Vazquez JA.** 2014. Development and antimicrobial susceptibility studies of in vitro monomicrobial and polymicrobial biofilm models with *Aspergillus fumigatus* and *Psuedomonas aeruginosa*. BMC Microbiol **14:** doi: 10.1186/1471-2180-14-53.

11. **Sutherland IW.** 2001. Biofilm exopolysaccharides: a strong and sticky framework. Microbiology **147:**3-9.

12. **Renault M, Cukkemane A, Baldus M.** 2010. Solid-state NMR spectroscopy on complex biomolecules. Angew Chem Int Ed **49:**8347-8357.

13. **Cegelski L, Hing AW, Kim SJ, Studelska DR, O'Connor RD, Mehta AK, Schaefer J.** 2002. Rotational-echo double resonance characterization of vancomycin mode of action in *S. aureus*. Biochemistry **41:**13053-13058.

14. **Curtis-Fisk J, Spencer RM, Weliky DP.** 2008. Native conformation at specific residues in recombinant inclusion body protein in whole cells determined with solid-state NMR spectroscopy. J Am Chem Soc **130:**12568-12569.

15. **Toke O, Cegelski L.** 2010. REDOR applications in biology: an overview, p 743-490. *In* McDermott AE, Polenova T (ed), Solid-state NMR studies of biopolymers. John Wiley & Sons Ltd, Chichester, UK.

16. **Kim SJ, Chang J, Singh M.** 2015. Peptidoglycan architecture of Gram-positive bacteria by solid-state NMR. Biochem Biophys Acta-Biomembranes **1848:**350-362.

17. **Yamamoto K, Caporini MA, Im SC, Waskell L, Ramamoorthy A.** 2015. Cellular solid-state NMR investigation of a membrane protein using dynamic nuclear polarization. Biochem Biophys Acta-Biomembranes **1848:**342-349.

18. **Ramamoorthy A.** 2009. Beyond NMR spectra of antimicrobial peptides: dynamical images at atomic resolution and functional insights. Solid state nuclear magnetic resonance **35:**201-207.

19. **Lim JY, May JM, Cegelski L.** 2012. Dimethyl sulfoxide and ethanol elicit increased amyloid biogenesis and amyloid-integrated biofilm formation in *E. coli*. Appl Environ Microbiol **78:**3369-3378.

20. **McCrate OA, Zhou X, Reichhardt C, Cegelski L.** 2013. Sum of the parts: composition and architecture of the bacterial extracellular matrix. J Mol Biol **425:**4286-4294.

21. **Reichhardt C, Fong JC, Yildiz F, Cegelski L.** 2015. Characterization of the *Vibrio cholerae* extracellular matrix: A top-down solid-state NMR approach. Biochim Biophys Acta **1848:**378-383.

22. **Reichhardt C, Cegelski L.** 2014. Solid-state NMR for bacterial biofilms. Mol Phys **112:**887-894.

23. **Hall-Stoodley L, Costerton JW, Stoodley P.** 2004. Bacterial biofilms: from the natural environment to infectious diseases. Nat Rev Microbiol **2:**95-108.

24. **Zarnowski R, Westler WM, Lacmbouh GA, Marita JM, Bothe JR, Bernhardt J, Lounes-Hadj Sahraoui A, Fontaine J, Sanchez H, Hatfield RD, Ntambi JM, Nett JE, Mitchell AP, Andes DR.** 2014. Novel entries in a fungal biofilm matrix encyclopedia. MBio **5:**e01333-01314.

25. **Oda K, Kakizono D, Yamada O, Iefuji H, Akita O, Iwashita K.** 2006. Proteomic analysis of extracellular proteins from *Aspergillus oryzae* grown under submerged and solid-state culture conditions. Appl Environ Microbiol **72:**3448-3457.

26. **Banerjee B, Greenberger PA, Fink JN, Kurup VP.** 1998. Immunological characterization of Asp f 2, a major allergen from *Aspergillus fumigatus* associated with allergic bronchopulmonary aspergillosis. Infect and Immun **66:**5175-5182.

27. **Schaefer J, Stejskal EO.** 1976. Carbon-13 nuclear magnetic resonance of polymers spinning at the magic angle. J Am Chem Soc **98:**1031-1032.

28. **Schaefer J, Stejskal EO, Buchdahl R.** 1975. High-resolution carbon-13 nuclear magnetic resonance study of some solid, glassy polymers. Macromolecules **8:**291-296.

29. **Fukamizo T, Kramer KJ, Mueller DD, Schaefer J, Garbow J, Jacob GS.** 1986. Analysis of chitin structure by nuclear magnetic resonance spectroscopy and chitinolytic enzyme digestion. Arch Biochem Biophys **249:**15-26.

30. **Bernard M, Latge JP.** 2001. *Aspergillus fumigatus* cell wall: composition and biosynthesis. Med Mycol **39:**S9-S17.

31. **Gullion T, Schaefer J.** 1989. Rotational-echo double-resonance NMR. J Magn Reson **81:**196-200.

32. **Cegelski L, Rice CV, O'Connor RD, Caruano AL, Tochtrop GP, Cai ZY, Covey DF, Schaefer J.** 2005. Mapping the locations of estradiol and potent neuroprotective analogues in phospholipid bilayers by REDOR. Drug Dev Res **66:**93-102.

33. **Gravelat FN, Beauvais A, Liu H, Lee MJ, Snarr BD, Chen D, Xu W, Kravtsov I, Hoareau CM, Vanier G, Urb M, Campoli P, Al Abdallah Q, Lehoux M, Chabot JC, Ouimet MC, Baptista SD, Fritz JH, Nierman WC, Latge JP, Mitchell AP, Filler SG, Fontaine T, Sheppard DC.** 2013. *Aspergillus* galactosaminogalactan mediates adherence to host constituents and conceals hyphal beta-glucan from the immune system. PLoS Pathog **9:**e1003575.

34. **Loussert C, Schmitt C, Prevost MC, Balloy V, Fadel E, Philippe B, Kauffmann-Lacroix C, Latge JP, Beauvais A.** 2010. In vivo biofilm composition of *Aspergillus fumigatus*. Cell Microbiol **12:**405-410.

592 35. **Elkins JG, Hassett DJ, Stewart PS, Schweizer HP, McDermott TR.** 1999. Protective
593 role of catalase in *Pseudomonas aeruginosa* biofilm resistance to hydrogen peroxide.
594 Appl Environ Microbiol **65:**4594-4600.
595 36. **Miller RA, Britigan BE.** 1997. Role of oxidants in microbial pathophysiology. Clin
596 Microbiol Rev **10:**1-18.
597 37. **Calera JA, Paris S, Monod M, Hamilton AJ, Debeaupuis J-P, Diaquin M, Lopez-**
598 **Medrano R, Leal F, Latge J-P.** 1997. Cloning and disruption of the antigenic catalase
599 gene of *Aspergillus fumigatus*. Infect Immun **65:**4718-4724.
600 38. **Jahn B, Langfelder K, Schneider U, Schindel C, Brakhage AA.** 2002. PKSP-
601 dependent reduction of phagolysosome fusion and intracellular kill of *Aspergillus*
602 *fumigatus* conidia by human monocyte-derived macrophages. Cell Microbiol **4:**793-803.
603 39. **Zhong J, Frases S, Wang H, Casadevall A, Stark RE.** 2008. Following fungal melanin
604 biosynthesis with solid-state NMR: biopolymer molecular structures and possible
605 connections to cell-wall polysaccharides. Biochemistry **47:**4701-4710.
606 40. **Banerjee A, Supakar S, Banerjee R.** 2014. Melanin from the nitrogen-fixing bacterium
607 *Azotobacter chroococcum*: a spectroscopic characterization. PLoS One **9:**e84574-e84574.
608 41. **Rajendran R, Williams C, Lappin DF, Millington O, Martins M, Ramage G.** 2013.
609 Extracellular DNA release acts as an antifungal resistance mechanism in mature
610 *Aspergillus fumigatus* biofilms. Eukaryot Cell **12:**420-429.

611

612

613 **FIGURE LEGENDS**

614

615 **Figure 1. Electron microscopy of *A. fumigatus* biofilm preparations and ECM protein**
616 **analysis.** (A-C) Scanning electron micrographs of intact *A. fumigatus* biofilm. (A) This lower
617 magnification micrograph shows the collection of hyphae associated with the *A. fumigatus*
618 biofilm formed in the modified version of RPMI medium used in this study. ECM connective
619 material is present between some of the hyphae, indicated by red arrows. (B) At higher
620 magnification, wide sheets of ECM are seen stretching between hyphae. (C) ECM that is closely
621 associated with hyphae can be observed at the highest resolution, with an apparent rough and
622 web-like coating, as shown in this image. (D) Transmission electron micrograph of isolated *A.*
623 *fumigatus* ECM. Fibrous material is indicated by a red arrow and vesicle-type structures are also
624 apparent. (E) SDS-PAGE protein gel of the *A. fumigatus* ECM. Five representative bands of the
625 SDS-soluble proteins (labeled 1-5) were excised and identified. Catalase B (Band 1: 79,910 Da)
626 and Asp f2 (Band 2: 32, 838 Da) were specifically identified. Bands 3-5 corresponded to
627 processed forms of these two proteins.
628
629 **Figure 2. Spectral comparisons of the carbon and nitrogen composition of the *A. fumigatus***
630 **biofilm and isolated ECM.** The $^{13}C$ CPMAS spectrum of the *A. fumigatus* intact biofilm sample
631 (cells plus ECM) contains major contributions from polysaccharides, consistent with the thick
632 hyphal cell walls (45,000 scans). The $^{13}C$ CPMAS spectrum of the ECM is consistent with a
633 material containing proteins (carbonyl and alpha carbon peaks), aromatic compounds (such as
634 melanin), and polysaccharides (48,000 scans). The spinning sidebands, which are a result of the
635 magic angle spinning and not representative of a specific carbon type, are indicated by asterisks.
636 The $^{15}N$ CPMAS spectrum of the whole biofilm contains a prominent peak centered at 122 ppm
637 indicative of amides. The smaller peaks are indicative of nitrogen-containing amino acid

638 sidechains (12,000 scans). The $^{15}N$ CPMAS spectrum of the ECM contains a similarly prominent
639 amide peak centered at 119 ppm plus other smaller peaks and nitrogen contributions (12,000
640 scans).
641
642 **Figure 3. Two-sample comparison of ECM carbon contributions.** $^{13}C$ CPMAS spectra of two
643 ECM samples revealed variations in the polysaccharide content. Analysis of the ECM samples
644 (left) isolated from their corresponding biofilms (right) identified differences in peaks uniquely
645 attributed to polysaccharides. The solid-line spectra are from Figure 2 and shown for direct
646 comparison with the dashed-line spectra from a second sample. The percentage of carbon
647 attributed to polysaccharide in the isolated ECM samples ranges from 20 to 43% of the total
648 carbon mass. The error bars represent the standard deviation. Corresponding differences were
649 observed in the intact biofilm. Carbon mass percentages in the ECM were determined by
650 quantitative CPMAS, performing CPMAS as a function of CP time for extrapolation. The intact
651 biofilm analysis is based on the CPMAS spectra shown.
652
653 **Figure 4. Spectroscopic selection of one-bond and two-bond C-N pairs.** $^{13}C\{^{15}N\}$REDOR
654 with a 1.6 ms evolution time identified carbons, and the percent of those carbons, that are
655 directly bonded to a nitrogen (64,000 scans for both $S_0$ and S). $^{13}C\{^{15}N\}$REDOR performed with
656 an evolution time of 8.95 ms revealed carbons that were within a two-bond proximity to nitrogen
657 (43,760 scans for both $S_0$ and S spectra).
658
659 **Figure 5. Phosphorus contributions to the ECM.** (A) $^{31}P$ CPMAS analysis of *A. fumigatus*
660 ECM. The $^{31}P$ CPMAS spectrum exhibited three overlapping chemical shifts and their associated

661 spinning sidebands, as indicted by ssb (9168 scans). (B) Spectroscopic selection of carbons near
662 to phosphorous. $^{13}C\{^{31}P\}$REDOR performed with an evolution time of 8.95 ms. The REDOR
663 difference spectrum (ΔS, red dashed spectrum) reveals the few carbon types that are proximate to
664 $^{31}P$ (38,000 scans for both $S_0$ and S spectra).

Eukaryotic Cell

EC

Eukaryotic Cell

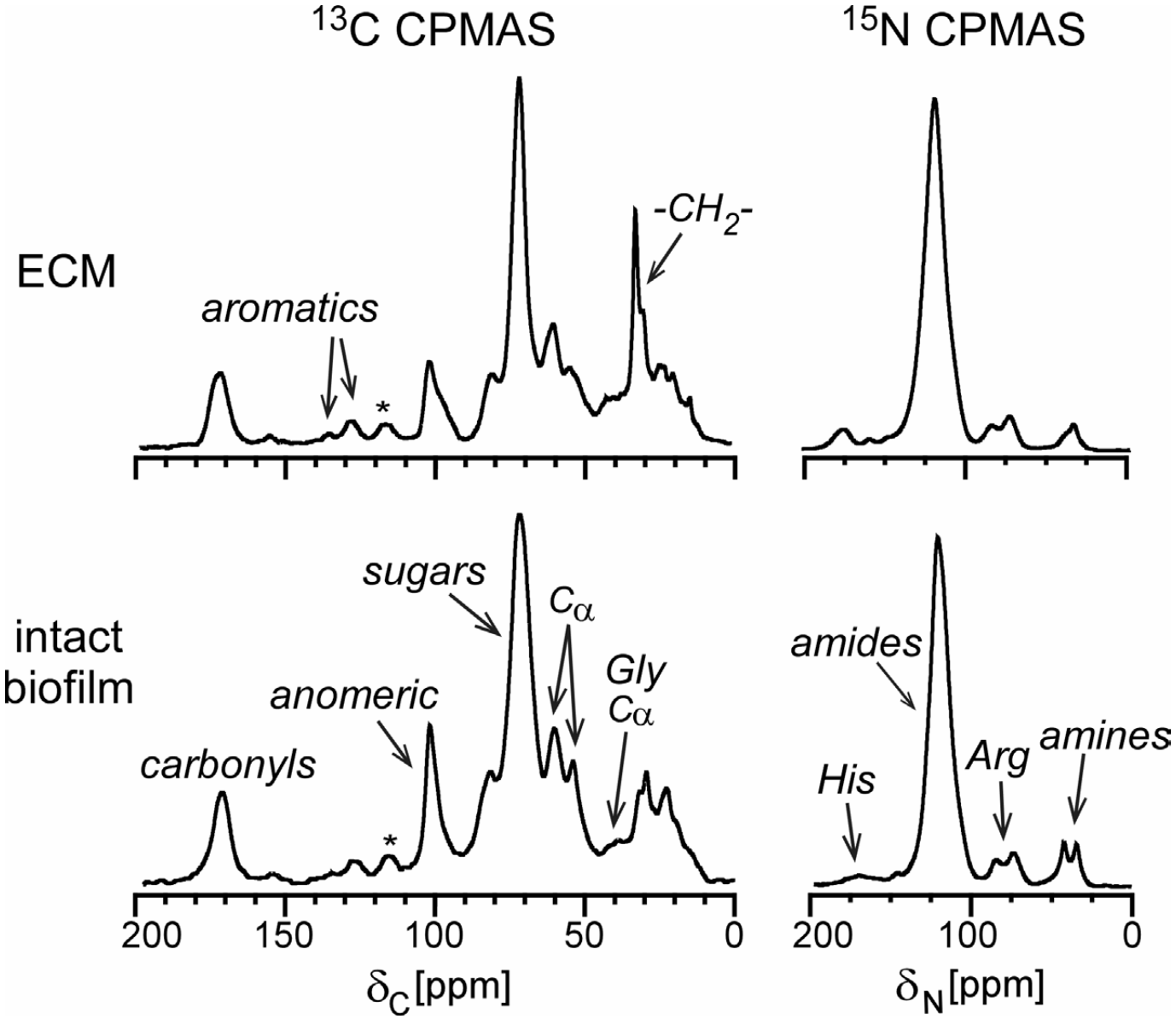

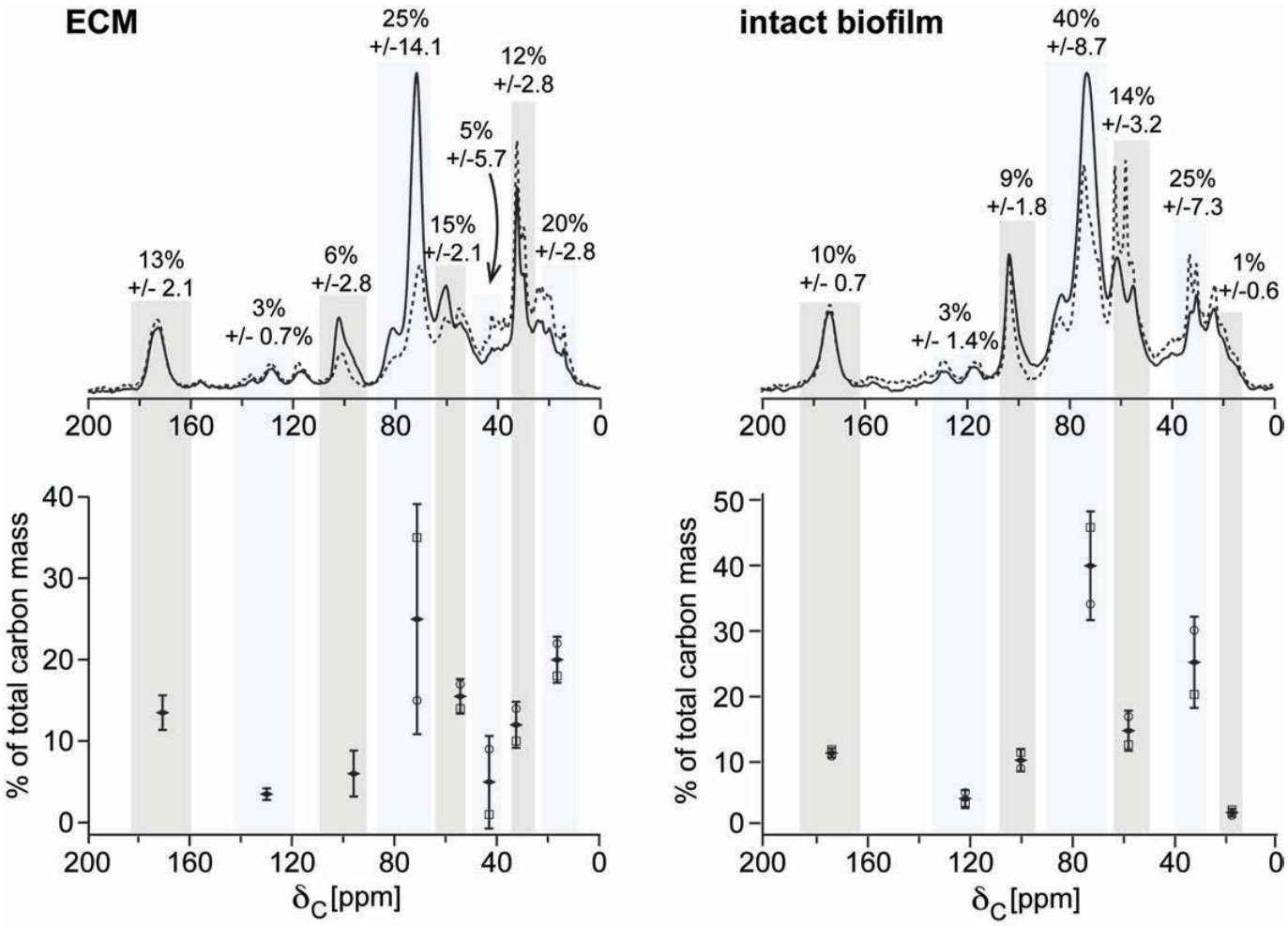

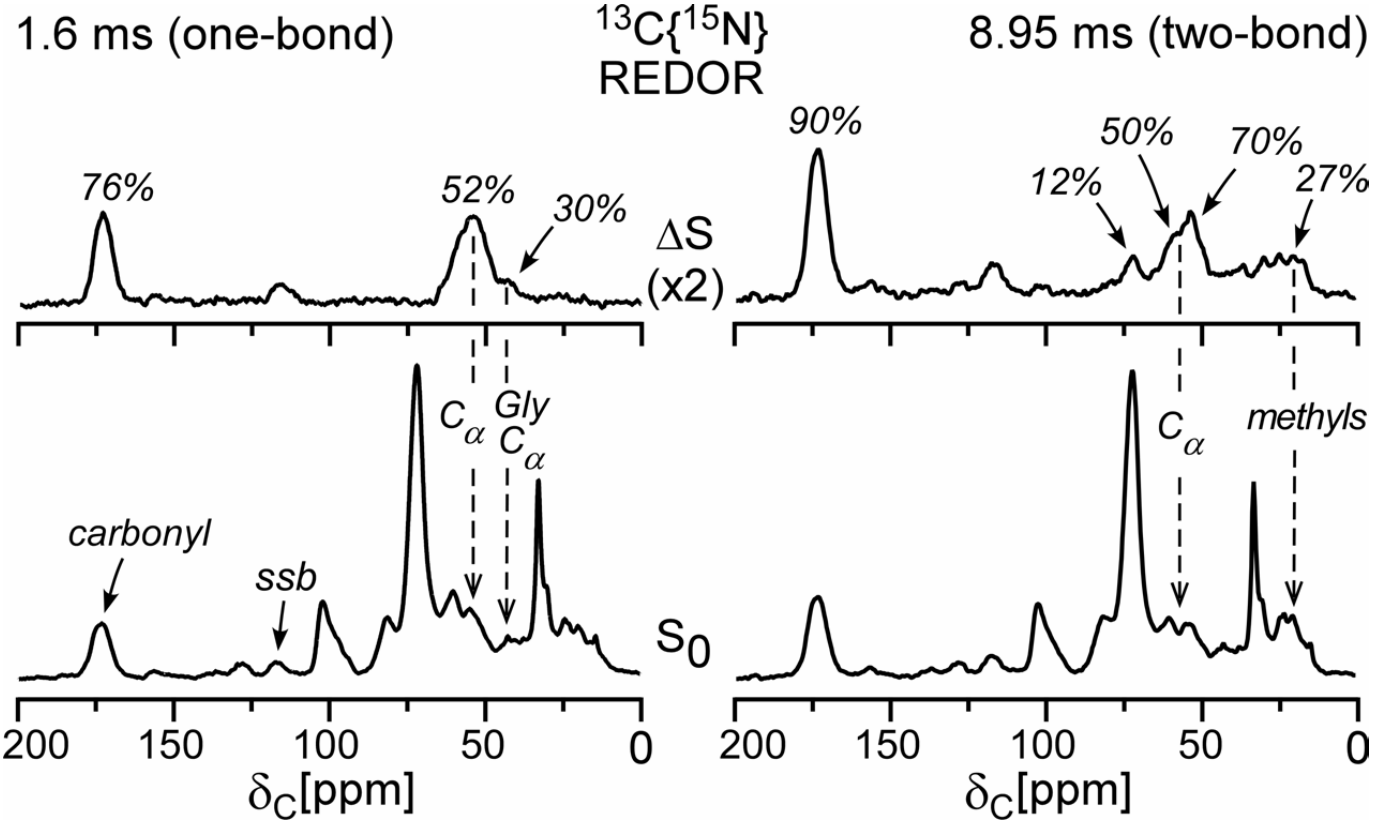






Eukaryotic Cell

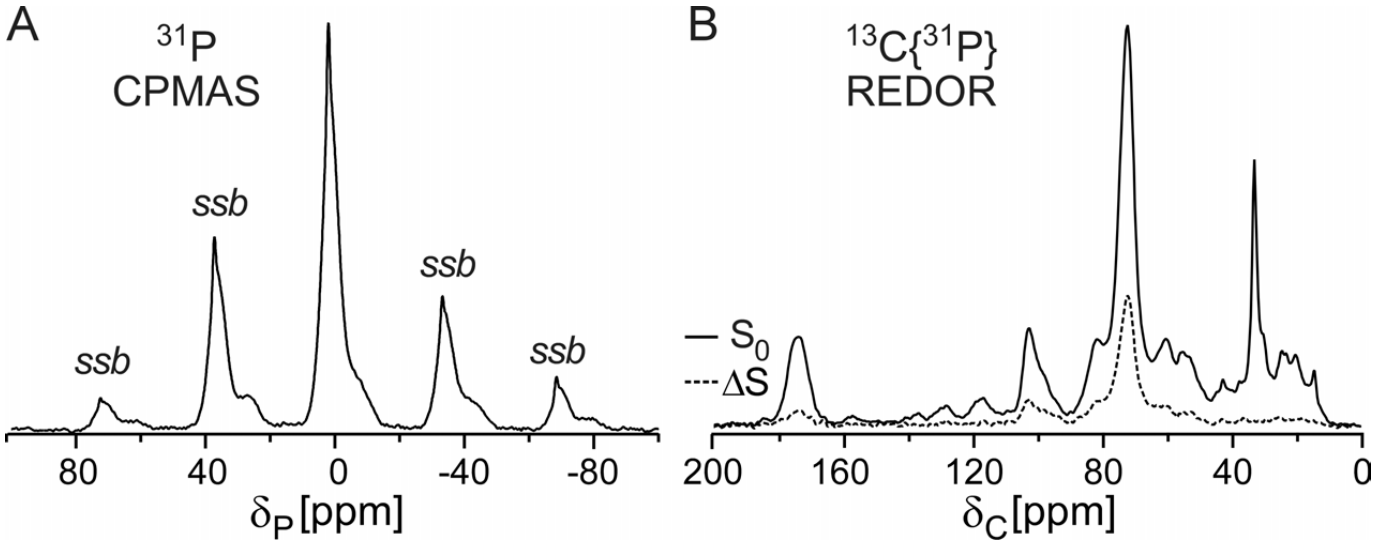

Defined carbon pools in the *A. fumigatus* ECM (grown in modified RPMI medium)

| **Chemical shift, $^{13}C$** | **173 ppm** | **130-160 ppm** | **94-104 ppm** | **60-80 ppm** | **50-60 ppm** | **38-43 ppm** | **33 ppm** | **12-25 ppm** |
|---|---|---|---|---|---|---|---|---|
| **Carbon type** | carbonyls | aromatics | anomerics | ring carbons | other $C_\alpha$ | Gly $C_\alpha$ | $CH_2$s | methyls |
| **Carbon mass (% of total)** | 12% | 3% | 8% | 35% | 7% | 0.3% | 10% | 18% |
| **Molecules** | amino acids, phospholipids, N- and O-acetyl modifications | melanin, amino acids | sugars | sugars | amino acids | Gly | amino acids, fatty acid chains | acetyl groups, amino acids |

**Representative chemical structures**

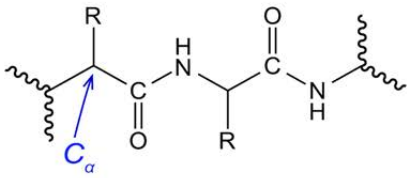


Peptide

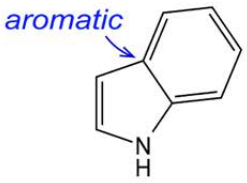


Indole
(melanin component)

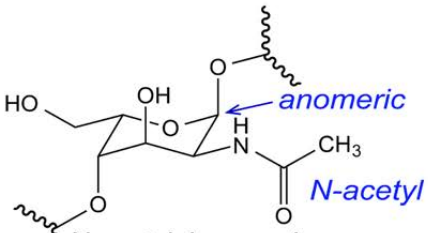


N-acetylglucosamine
(modified sugar)





Eukaryotic Cell